

1 **Meteorological constraints on oceanic halocarbons above the Peruvian**
2 **Upwelling**

3

4 **S. Fuhlbrügge¹, B. Quack¹, E. Atlas², A. Fiehn¹, H. Hepach¹, K. Krüger³**

5 [1] GEOMAR | Helmholtz Centre for Ocean Research Kiel

6 [2] Rosenstiel School for Marine and Atmospheric Sciences, Miami, Florida

7 [3] University of Oslo, Oslo, Norway

8 Correspondence to: K. Krüger (kirstin.krueger@geo.uio.no)

9

10 **Abstract**

11 Halogenated very short lived substances (VSLS) are naturally produced in the ocean and
12 emitted to the atmosphere. Recently, oceanic upwelling regions in the tropical East Atlantic
13 were identified as strong sources of brominated halocarbons to the atmosphere. During a
14 cruise of R/V METEOR in December 2012 the oceanic sources and emissions of various
15 halogenated trace gases and their mixing ratios in the marine atmospheric boundary layer
16 (MABL) were investigated above the Peruvian Upwelling for the first time. This study
17 presents novel observations of the three VSLS bromoform, dibromomethane and methyl
18 iodide together with high resolution meteorological measurements and Lagrangian transport
19 modelling. Although relatively low oceanic emissions were observed, except for methyl
20 iodide, surface atmospheric abundances were elevated. Radiosonde launches during the
21 cruise revealed a low, stable MABL and a distinct trade inversion above acting both as strong
22 barriers for convection and trace gas transport in this region. Significant correlations between
23 observed atmospheric VSLS abundances, sea surface temperature, relative humidity and
24 MABL height were found. We used a simple source-loss estimate to identify the contribution
25 of oceanic emissions to observed atmospheric concentrations which revealed that the
26 observed marine VSLS abundances were dominated by horizontal advection below the trade
27 inversion. The observed VSLS variations can be explained by the low emissions and their
28 accumulation under different MABL and trade inversion conditions. This study confirms the
29 importance of oceanic upwelling and trade wind systems on creating effective transport

30 barriers in the lower atmosphere controlling the distribution of VLSL abundances above
31 ocean upwelling regions.

32

33 **1. Introduction**

34 Short-lived halocarbons from the oceans contribute to reactive atmospheric halogens, which
35 are involved in tropospheric and stratospheric ozone depletion, aerosol formation, and other
36 chemical cycles, influencing the fate of pollutants and climate (McGivern et al., 2000;Saiz-
37 Lopez and von Glasow, 2012;Simpson et al., 2015). Recent studies have identified open
38 ocean upwelling areas in the Atlantic as large source regions for a number of brominated and
39 iodinated oceanic trace gases (Quack et al., 2004;Quack et al., 2007;O'Brien et al.,
40 2009;Raimund et al., 2011;Hepach et al., 2015a). Their sources are related to biological and
41 chemical processes in the productive waters of the upwelling. The compounds are emitted
42 from the ocean and are horizontally transported and vertically mixed in the marine
43 atmospheric boundary layer (MABL) (Carpenter et al., 2010). In the Mauritanian upwelling,
44 it was found that besides oceanic sources meteorological conditions strongly influenced the
45 atmospheric mixing ratio of the marine compounds bromoform (CHBr_3), dibromomethane
46 (CH_2Br_2) and also methyl iodide (CH_3I) (Hepach et al., 2014). Especially the combination of
47 a pronounced low MABL above cold upwelling waters with high concentrations and
48 emissions of the compounds caused elevated atmospheric mixing ratios. In return, these
49 atmospheric mixing ratios also reduce the marine emissions through a decrease of the sea-air
50 concentration gradient (Fuhlbrügge et al., 2013). Similar relationships would be expected for
51 other oceanic upwelling areas, where not only the oceanic emissions, but also meteorological
52 conditions in the lowermost atmosphere, i.e., the height, type and structure of the boundary
53 layer and trade inversion, determine the VLSL contribution to atmospheric chemical
54 processes. The intense oceanic upwelling in the Southeast Pacific off the coast of Peru
55 transports large amounts of subsurface waters to the ocean surface and creates one of the
56 highest productive oceanic regions worldwide (Codispoti et al., 1982). The Peruvian
57 Upwelling is therefore a potentially intense source region for halogenated VLSL, e.g.
58 bromoform, dibromomethane and methyl iodide (Yokouchi et al., 1999;Butler et al.,
59 2007;Carpenter et al., 2009). Indeed, Schönhardt et al. (2008) detected elevated IO columns
60 during September and November 2005 along the Peruvian coast with the SCIAMACHY
61 satellite instrument and implied elevated iodine source gases from the Peruvian Upwelling.

62 Although, recent studies investigated halocarbons in the East Pacific (Yokouchi et al.,
63 2008;Mahajan et al., 2012;Saiz-Lopez et al., 2012;Gómez Martin et al., 2013;Liu et al., 2013)
64 few studies concentrated on the Peruvian Upwelling in the Southeast Pacific. Only
65 measurements of methyl iodide exist in this region, revealing atmospheric abundances of 7
66 ppt (Rasmussen et al., 1982). Observations of bromocarbons above the Peruvian Upwelling
67 are lacking.

68 In this study we present a high resolution dataset of meteorological parameters, oceanic
69 concentrations, emissions and atmospheric abundances of VSLS along the Peruvian coast and
70 in the Upwelling. Not much is known of the oceanic source strength of the VSLS and the
71 meteorological influence on the marine trace gas distribution and abundances in this region.
72 The goal of this study is to assess the influence of oceanic upwelling and meteorological
73 conditions on the atmospheric VSLS abundances above the Peruvian Upwelling, and the
74 contribution of the local oceanic emissions to MABL and free tropospheric VSLS
75 concentrations.

76 The paper is structured as following. Chapter 2 gives an overview of the data and methods we
77 use in this study. Chapter 3 presents the results from our atmospheric and oceanic
78 observations and analyses the contribution from oceanic VSLS emissions to the MABL, as
79 well as meteorological constrains on the observations. Chapter 4 discusses the results, before
80 the study is summarized in Chapter 5.

81

82 **2. Data and Methods**

83 The cruise M91 on R/V METEOR from December 01 to 26, 2012 started and ended in Lima,
84 Peru. The ship reached the most northern position during the cruise on December 03, 2012 at
85 5° S. In the following three weeks the ship headed southward and reached its southern most
86 position at 16° S on December 21, 2012. During this time the track alternated between open
87 ocean sections and sections very close to the Peruvian coast in the cold upwelling waters to
88 collect coastal as well as open ocean data. Diurnal variations were observed during 6 stations
89 along the cruise track.

90

91 **2.1 Meteorological observations**

92 Meteorological measurements of surface air temperature (SAT), sea surface temperature
93 (SST), relative humidity, air pressure, wind speed and direction were taken every second at
94 about 25 m height on R/V METEOR and averaged to 10 minute intervals for our
95 investigations. Atmospheric profiles of temperature, wind and humidity were obtained by 98

96 radiosonde launches at standard UTC time (0, 6, 12, 18 UTC) and additionally 3 hourly
97 during the diurnal stations along the cruise track, using Vaisala RS92 radiosondes. Due to
98 permission limitations, radiosondes could not be launched within 12 nautical miles of the
99 Peruvian coast. The collected radiosonde data was integrated in near real time into the Global
100 Telecommunication System (GTS) to improve meteorological reanalysis (e.g. ERA-Interim)
101 and operational European Centre for Medium Range Weather Forecast models (opECMWF).

102

103 **2.2 MABL height**

104 The radiosonde data are used to identify the height of the MABL, which is the atmospheric
105 surface layer above the ocean in which trace gas emissions are mixed horizontally on a short
106 time scale of an hour or less by convection and turbulence (Stull, 1988). Two different kinds
107 of MABL can be distinguished, the convective and the stable MABL, which can be
108 characterized by the gradient of the virtual potential temperature θ_v . A negative or neutral
109 gradient reveals an unstable convective layer, while a positive gradient reveals a stable
110 atmospheric layer. In case of an increase of the virtual potential temperature near the surface,
111 mixing in the MABL is suppressed. The upper limit of the convective MABL is set by a
112 *stable layer*, e.g., a temperature inversion or a significant reduction in air moisture and is
113 typically found above open ocean regions between 100 m and 3 km height (Stull,
114 1988;Seibert et al., 2000). For the determination of this *stable layer* above the convective
115 MABL, we use the practical approach described in Seibert et al. (2000) and compute the
116 virtual potential temperature during the radiosonde ascent whose increase with altitude
117 indicates the base of a *stable layer*. In this study the base of this *stable layer* increased by half
118 of this *stable layer* depth is the definition for the MABL height. Over oceanic upwelling
119 regions this stable layer can even descend to the ocean surface (e.g. Höflich et al., 1972 and
120 Fuhlbrügge et al., 2013).

121

122 **2.2.1 Relative humidity**

123 Estimates for atmospheric surface stability and MABL conditions in oceanic upwelling
124 region can also be obtained from variations of the surface humidity. While the absolute
125 humidity determines the amount of water in a specific volume of air, the relative humidity is
126 the ratio of the partial pressure of water vapour to the equilibrium vapour pressure at the
127 observed temperature. Variations of the SAT therefore directly influence the relative
128 humidity at the surface. A decrease of the SAT due to cold upwelling water leads to an
129 increase of the relative humidity, while the absolute humidity stays constant or even

130 decreases due to condensation of water vapour once the relative humidity reaches 100 % and
131 the air is saturated with water vapour. An elevated relative humidity in this oceanic region
132 therefore points to stable layers with suppressed mixing of surface air and to a low and stable
133 MABL height.

134

135 **2.2.2 Estimation of MABL height above the upwelling**

136 To estimate the MABL height above upwelling areas close to the coast, where radiosonde
137 launches were permitted (Section 2.1) a multiple linear regression was applied. Using
138 observed meteorological parameters revealing significant correlations (see Section 3.5) with
139 the observed MABL height, relative humidity (x_1), SAT (x_2), SST (x_3) and wind speed (x_4),
140 along the cruise we obtained the following Eq. 1:

141

$$114 \text{ MABL height} = b_1x_1 + b_2x_2 + b_3x_3 + b_4x_4 \quad (\text{Eq. 1})$$

with $b_1 = -0.0117$; $b_2 = 0.0202$; $b_3 = 0.0467$; $b_4 = 0.0089$

142

143 **2.3 Atmospheric VSLs measurements**

144 A total of 198 air samples were collected 3 hourly during the cruise at about 20 m height on
145 the 5th superstructure deck of R/V METEOR using a portside jib of 5 – 6 m. The air samples
146 were pressurized to 2 atm in pre-cleaned stainless steel canisters with a metal bellows pump
147 and were analysed at the Rosenstiel School for Marine and Atmospheric Sciences (RSMAS,
148 Miami, Florida) within 6 months after the cruise. Details about the analysis, the instrumental
149 precision and the preparation of the samples are described in Schauflier et al. (1999) and
150 Fuhlbrügge et al. (2013). The atmospheric mixing ratios were calculated with a NOAA
151 standard (SX3573) from GEOMAR.

152

153 **2.4 Oceanic concentrations and sea – air flux**

154 102 water samples were taken 3 hourly at a depth of 6.8 m from a continuously working
155 water pump in the hydrographic shaft, an opening in the base of the ship hull of R/V Meteor,
156 after December 9, 2012. The samples were then analysed for bromoform, dibromomethane
157 and methyl iodide and other halogenated trace gases by a purge and trap system, attached to a
158 gas chromatograph combined with an ECD (electron capture detector) with a precision of 10
159 % determined from duplicates. The approach is described in detail by Hepach et al. (2014).

160

161 **2.4.1 Sea – air flux**

162 The sea – air flux (F) of bromoform, dibromomethane and methyl iodide is calculated with k_w
163 as transfer coefficient and Δc as concentration gradient between the water and equilibrium
164 water concentration determined from the atmospheric concentrations (Eq. 2). The transfer
165 coefficient was determined by the air – sea gas exchange parameterization of Nightingale et
166 al. (2000) after a Schmidt number (Sc) correction for the three gases (Eq. 3).

$$F = k_w \cdot \Delta c \quad (\text{Eq. 2})$$

$$k_w = k_{CO_2} \cdot \frac{Sc^{-\frac{1}{2}}}{600} \quad (\text{Eq. 3})$$

169
170 Details on deriving the air – sea concentration gradient and emissions are further described in
171 Hepach et al. (2014) and references therein.

172
173 **2.5 Trajectory calculations**

174 The Lagrangian Particle Dispersion Model FLEXPART of the Norwegian Institute for Air
175 Research in the Department of Atmospheric and Climate Research (Stohl et al., 2005) was
176 used to analyse the air mass origins and the transport of surface air masses along the cruise
177 track to the free troposphere (Stohl et al., 1998;Stohl and Trickl, 1999). The model includes
178 moist convection and turbulence parameterizations in the atmospheric boundary layer and
179 free troposphere (Stohl and Thomson, 1999;Forster et al., 2007). We use the ECMWF
180 (European Centre for Medium-Range Weather Forecasts) reanalysis product ERA-Interim
181 (Dee et al., 2011) with a horizontal resolution of $1^\circ \times 1^\circ$ and 60 vertical model levels as
182 meteorological input fields, providing air temperature, horizontal and vertical winds,
183 boundary layer height, specific humidity, as well as convective and large scale precipitation
184 with a 6 hourly temporal resolution. Due to the spatial resolution of ERA-Interim data along
185 the Peruvian coast defining the land-sea mask of our trajectory calculations, 98 out of 140
186 release points for the forward and backward trajectory calculations were analysed along the
187 cruise track. At each these release points 10,000 forward and 50 backward trajectories were
188 launched from the ocean surface within ± 30 minutes and ~ 20 m distance to the ship position.
189 Time and position of the release events are synchronized with air samples taken on R/V
190 METEOR (Section 2.3).

191

192 **2.6 Oceanic contribution to MABL VSLS abundances**

193 To obtain an estimate of the contribution of local oceanic sources to the atmospheric mixing
194 ratios in the lowermost atmosphere above the Peruvian upwelling we apply a mass balance
195 concept to the oceanic emissions, to the time scales of air mass transport and to the chemical
196 loss (Fuhlbrügge et al., 2015). First we define a box above each release event with a size of
197 $\sim 400 \text{ m}^2$ around the measurement location and the height of the MABL and assume a steady-
198 state observed VSLS mixing ratio within the box (Figure 1). During each trajectory release
199 event we assume the specific sea-air flux to be constant and the emissions to be
200 homogeneously mixed within the box. Then the contribution of the sea-air flux is computed
201 as the ratio of the VSLS flux from the ocean into the MABL (in mol per day) and the total
202 amount of VSLS in the box (in mol) and is defined as the Oceanic Delivery (OD) and OD is
203 given in percentage per day. In addition to the delivery of oceanic VSLS to the box, the loss
204 of VSLS out of the box into the free troposphere is defined as the CONvective Loss (COL)
205 and is derived from the mean residence time derived from the FLEXPART trajectories in the
206 box during each release event. Since this process is a loss process, COL is given as a negative
207 quantity and in percentage per day. The chemical degradation of VSLS by OH and photolysis
208 in the MABL is considered by the chemical lifetime of each compound in the MABL. We use
209 lifetimes of 16 days for bromoform and 60 days for dibromomethane (Hossaini et al., 2010)
210 and 3 days for methyl iodide (R. Hossaini, personal communication), representative for the
211 tropical boundary layer. The Chemical Loss (CL) acts as loss process as well and is given as
212 a negative quantity in percentage per day. We further assume a steady state in the box. OD,
213 COL and CL must therefore be balanced by an advective transport of air masses in and out of
214 the box. The change of the VSLS through advective transport is defined as Advective
215 Delivery (AD) and given in percentage per day.

216 By ratioing OD to COL, we estimate an Oceanic Delivery Ratio (ODR) (Eq. 4):

217

$$ODR = \frac{OD [\%d^{-1}]}{-COL [\%d^{-1}]} = \frac{Sea-Air \text{ flux contribution } [\%d^{-1}]}{Loss \text{ of box air to the FT } [\%d^{-1}]} \quad (\text{Eq. 4})$$

218

219 Similarly, the Chemical Loss in the box (CL) and the change in VSLS due to advection (AD)
220 are related to COL to get the Chemical Loss Ratio (CLR) and the Advective Delivery Ratio
221 (ADR) with $ADR = 1 - CLR - ODR$. Since CL, OD and AD are divided by $-COL$, ratios for
222 source processes are positive and negative for loss processes (Fuhlbrügge et al., 2015).

223

224 **3. Observations on R/V METEOR**

225 **3.1. Meteorological observations**

226 The Peruvian coast is dominated by the southern hemisphere trade wind regime with
227 predominantly southeast winds (Figure 2). The Andes, which are known to act as a barrier to
228 zonal wind in this region, affect the horizontal air mass transport along the coast (Figure 2b-
229 d). The steeply sloping mountains at the coast form strong winds parallel to the South
230 American coastline (Garreaud and Munoz, 2005), leading to distinct wind-driven oceanic
231 upwelling of cold water along the coast. The 10-day backward trajectories reveal
232 predominantly near-shore air masses with coastal influence and marine air masses (Figure 2).
233 The average wind direction observed on R/V Meteor during the cruise is $160^\circ \pm 34^\circ$ (mean
234 $\pm \sigma$) with a moderate average wind speed of $6.2 \pm 2.2 \text{ ms}^{-1}$ (Figure 3b). ERA-Interim reveals
235 similar winds along the cruise track with a mean wind speed of $5.6 \pm 1.8 \text{ ms}^{-1}$ and a mean
236 wind direction of $168^\circ \pm 21^\circ$ (not shown here). The divergence of the wind driven Ekman
237 transport along the Peruvian coast leads to the observed oceanic upwelling of cold waters.
238 The most intense upwelling is observed for several times near the coast where both, SST and
239 SAT rapidly drop from $19 - 22^\circ \text{C}$ to less than 18°C (Figure 3a). The impact of the cold
240 upwelling water on the observed air masses is also visible in the observed humidity fields
241 (Figure 3c). Here, the decreasing SAT reduces the amount of water vapour that the surface air
242 is able to contain, leading to an increase of the relative humidity. The decreasing SAT and
243 increasing relative humidity above the oceanic upwelling indicate a stable atmospheric
244 surface layer with suppressed vertical mixing. The absolute humidity stays constant or even
245 decreases above the oceanic upwelling due to condensation of water vapour when surface air
246 cools and becomes saturated, which coincides with fog observations on the ship above the
247 upwelling regions. A decrease of the absolute humidity outside the upwelling points to a
248 change in advected air masses for example between December 9 and 11, but also on
249 December 19, 2012 (Figure 3c).

250

251 **3.2. VLSL observations and oceanic emissions**

252 Surface bromoform concentrations in the Peruvian upwelling are generally lower during the
253 cruise compared to the Mauritanian upwelling while dibromomethane surface water
254 concentrations are comparable. However methyl iodide concentrations are almost 8 times
255 higher than in the Mauritanian upwelling (Figure 3d, Table 1, Hepach et al., 2014). Samples
256 taken in the upwelling areas show elevated concentrations compared to the open ocean for all

257 compounds. For further discussion on the distribution of the oceanic halocarbons, see Hepach
258 et al. (2016, submitted to ACPD).

259 Atmospheric mixing ratios of bromoform are on average 2.91 ± 0.68 ppt (Table 1).
260 Dibromomethane mixing ratios of 1.25 ± 0.26 ppt are low and show a similar temporal
261 pattern with bromoform (Table 3). Mixing ratios of both compounds are significantly lower
262 above the Peruvian upwelling compared to observations above the Mauritanian upwelling,
263 while methyl iodide mixing ratios are comparable (Fuhlbrügge et al., 2013). Elevated mixing
264 ratios for all three compounds are generally found above intense cold oceanic upwelling
265 regions close to the Peruvian coast (Figure 3e). While the bromocarbons double above the
266 upwelling, methyl iodide mixing ratios increase up to 5-fold, showing its stronger
267 accumulation in the low boundary layer.

268 The concentration ratio of dibromomethane and bromoform can be used as an indicator of
269 fresh bromocarbon sources along coastal areas. Low ratios of about 0.1 have been observed at
270 coastal source regions and are interpreted as the emission ratios of macro algae (Yokouchi et
271 al., 2005; Carpenter et al., 2003). The applied shorter mean lifetime of bromoform (15 days)
272 in contrast to dibromomethane (94 days) in the boundary layer after Carpenter et al. (2014)
273 leads to an increase of the ratio during transport as long as the air mass is not enriched with
274 fresh bromoform. A general decrease of the concentration ratio is found from the North to the
275 South during the cruise (Figure 3f), implying relatively remote air masses in the North and an
276 intensification of fresh sources towards the south, which is also reflected by the elevated
277 water concentrations. Atmospheric methyl iodide measurements along the cruise track reveal
278 a mean mixing ratio of 1.54 ± 0.49 ppt, which, similar to the two bromocarbons, maximizes
279 over the coastal upwelling regions (Figure 3e).

280 Oceanic emissions during the cruise were calculated from the synchronized measurements of
281 sea water concentrations and atmospheric mixing ratios, sea surface temperatures and wind
282 speeds, measured on R/V METEOR (Section 2.4.1). Oceanic concentrations and atmospheric
283 mixing ratios of each compound are weakly or not at all correlated ($R_{\text{bromoform}} = 0.00$,
284 $R_{\text{dibromomethane}} = 0.29$ and $R_{\text{methyl iodide}} = 0.34$). Mean sea-air fluxes of the bromocarbons during
285 the cruise are very low with 117 ± 492 pmol m⁻² hr⁻¹ for bromoform and 245 ± 299 pmol m⁻²
286 hr⁻¹ for dibromomethane, but for methyl iodide the fluxes are elevated with 856 ± 623 pmol
287 m⁻² h⁻¹ (Figure 3g, Table 1). Further investigations of the distributions and sources of
288 iodinated compounds during this cruise are carried out by Hepach et al. (2015b).

289

290 **3.3. Lower atmosphere conditions**

291 The relative humidity shows a strong vertical gradient from over 75 % to less than 50 % at ~1
292 km height (Figure 4a) which indicates an increase of the atmospheric stability with height due
293 to suppressed mixing. This convective barrier, known as the trade inversion (Riehl, 1954,
294 1979;Höflich, 1972), is also reflected in the meridional wind (Figure 4b). Below ~1 km
295 altitude the Southeast trade winds create a strong positive meridional wind component, also
296 visible in the forward trajectories (Figure 2c-d). The flow of air masses in the Hadley Cell
297 back to the subtropics causes a predominantly northerly wind above ~1 km height. The
298 intense increase of θ_v in combination with the relative humidity decrease and the wind shear
299 at ~1 km height identifies this level as a strong vertical transport barrier (Figure 4c). Above
300 the cold upwelling water, temperature inversions create additional stable layers above the
301 surface, leading to very low MABL heights of < 100 m, e.g., on December 03, 08 or 17, 2012
302 and to a reduced vertical transport of surface air. The mean MABL height from the
303 radiosonde observations is 370 ± 170 m (ERA-Interim 376 ± 169 m). The relative humidity,
304 SAT, SST and wind speed are good indicators for the MABL conditions in this oceanic
305 region and these meteorological parameters show significant correlations with the observed
306 MABL height (Table 3). Thus, we use a multiple linear regression based on these parameters
307 to estimate the MABL height above the coastal upwelling (Section 2.2.2). The regressed
308 MABL heights above the cold upwelling regions are 158 ± 79 m and go down to even 10 m
309 as was previously observed above the Mauritanian Upwelling (Fuhlbrügge et al., 2013). With
310 the regressed MABL heights, the mean MABL height during the cruise decreases to $307 \pm$
311 177 m. The stable atmospheric conditions from the surface to the trade inversion lead to
312 strong transport barriers and to a suppressed transport of surface and MABL air into the free
313 troposphere (Figure 4d).

314 We interpret the observations as the following. In the region of the Peruvian Upwelling,
315 compounds emitted from the ocean and observed at the marine surface are first
316 homogeneously distributed within the MABL during a couple of hours, before advection
317 transport them further within the second transport barrier of the lowermost atmosphere the
318 trade wind inversion. For air masses above or close to oceanic upwelling regions, the MABL
319 height is the first weak transport barrier on short time scales (hours), while the trade
320 inversions acts as the second more pronounced barrier for vertical transport on long time
321 scales (days).

322

323 **3.4. Contribution of oceanic emissions to observed VSLS abundances in the** 324 **MABL**

325 We estimate the contribution of oceanic emissions to mixing ratios within the MABL and
326 below the trade inversion with a VSLS source-loss estimate (Table 2). The loss of VSLS out
327 of the MABL box is -351.0 \% d^{-1} and equal for all compounds, since it is computed from the
328 loss of trajectories out of the box. The loss is based on a mean residence time of the
329 FLEXPART trajectories of 7 hours in the observed MABL height during the cruise. The ratio
330 of the OD of each compound and the COL results in the particular ODR. The ODR reveals
331 that on average only 3 % of the observed atmospheric bromoform in the MABL origins from
332 nearby oceanic emissions and that 99 % are advected. Local oceanic emissions of
333 dibromomethane contribute about 10 % of the observed abundances in the MABL, while
334 methyl iodide emissions contribute with 28 %, which is far less compared to observations in
335 other source regions with high convection as in the South China and Sulu Seas (Fuhlbrügge
336 et al., 2015). Generally, the low ODRs along the cruise track are caused by the relatively low
337 oceanic emissions. Since the observed atmospheric concentrations cannot be explained by the
338 local oceanic emissions advection leads to the background concentrations of bromoform and
339 methyl iodide. According to the backward trajectories, potential source regions may be found
340 closer to the coast and to the South. The elevations of the atmospheric mixing ratios above
341 the cold coastal upwelling can partly be explained by accumulation of local oceanic
342 emissions in the stable low MABL. However, as the emissions appear generally not strong
343 enough, except for methyl iodide, to explain the mixing ratios, the contribution of coastal
344 sources is very likely (Figure 2b). While the surface air masses can leave the MABL within
345 hours, they are suppressed from entering the free troposphere through the trade inversion
346 barrier. Adapting an average trade inversion height of 1.1 km as the transport barrier for
347 surface air masses into the free troposphere reveals an average residence time of the
348 FLEXPART trajectories of 48 hrs below this trade inversion height. The atmospheric VSLS
349 below the trade inversion originate to 11 % from oceanic emissions (ODR) for bromoform, to
350 33 % for dibromomethane and to 92 % for methyl iodide. The increased residence time of air
351 masses below the trade inversion, reflected by the FLEXPART trajectories, leads to a
352 stronger enrichment of air masses with VSLS from the oceanic emissions, reflected by OD,
353 compared to the MABL box. However, the low sea-air fluxes of bromoform and
354 dibromomethane are by far not strong enough to lead to the observed mixing ratios. These
355 numbers imply that observed VSLS concentrations are advected below the trade inversion in
356 the more open ocean regions during the cruise. An overall discussion is given in Section 4.

357

358 **3.5. Meteorological constrains on atmospheric VSLS in the MABL**

359 Fuhlbrügge et al. (2013) identified the influence of meteorological conditions, in particular of
360 MABL height variations on VSLS abundances in the tropical Northeast Atlantic above the
361 Mauritanian Upwelling, and suggested a general correlation of MABL conditions and VSLS
362 abundances over oceanic upwelling regions. Indeed, we also find significant high correlations
363 between meteorological parameters and the abundances of bromoform, dibromomethane and
364 methyl iodide (Table 3) along the Peruvian coast. The predominantly moderate winds during
365 the cruise are negatively correlated with the atmospheric VSLS and positively correlated with
366 the MABL height. This shows that VSLS abundances tend to be elevated during periods of
367 lower wind speeds which occur also lead to reduced mixing of surface air and therefore to
368 lower MABL heights, in particular above the coastal upwelling events on December 11, 15-
369 17 and 24, 2012, where local sources could accumulate even more. SAT and SST both are
370 negatively correlated with atmospheric VSLS, since elevated atmospheric VSLS mixing
371 ratios are generally found close to the oceanic upwelling regions with low SATs and SSTs. In
372 these regions the decrease of the SATs leads to an increase of the relative humidity (section
373 3.1), resulting in a significantly high correlation between the surface relative humidity and
374 the VSLS. Since SAT and SST impact the MABL, which affects the relative humidity, these
375 correlation coefficients are co-correlated with each other. Correlation coefficients between
376 the MABL height and the VSLS are slightly lower (Table 3). A principle component analysis
377 of the parameters in Table 3 furthermore underlined a strong connection between SAT, SST,
378 MABL height, relative humidity and atmospheric mixing ratios of bromoform and
379 dibromomethane (not shown here).

380 The results reveal that the MABL properties (height and stability) during M91 influence the
381 VSLS abundances at the marine surface, although not as distinct as above the Mauritanian
382 Upwelling during the DRIVE campaign (Fuhlbrügge et al., 2013). A comparison between the
383 observations from this campaign and DRIVE (Figure 5) shows that the lower variance of
384 observations during M91 may explain the lower correlation. Generally higher emissions and
385 occasional lower and even more stable MABL-heights during DRIVE can explain up to
386 100% of the atmospheric abundances (Fuhlbrügge et al., 2013; Hepach et al., 2014), while
387 during M91 the observed elevations could only partly be explained by the local oceanic
388 emissions.

389

390 **4. Discussion**

391 The observations reveal a significant correlation between the MABL height and atmospheric
392 VSLs abundances above the Peruvian Upwelling. However, the correlation coefficients
393 between the determined MABL height and the atmospheric VSLs are not as high as above
394 the Mauritanian Upwelling during the DRIVE campaign (Fuhlbrügge et al., 2013). Reasons
395 might be the large area of the investigated region in the Northeast Atlantic Ocean during the
396 DRIVE campaign (25° latitude x 10° longitude) in contrast to this study along the Peruvian
397 coast (12° latitude x 2° longitude). M91 observations therefore involve less variability of
398 covered oceanic regimes of open ocean and coastal upwelling, VSLs concentrations and
399 meteorological parameters, in particular of the MABL height, than the DRIVE observations.
400 The Andes along South America lead to predominantly Southerly winds along the West coast
401 line with minor continental influence, while the Mauritanian Upwelling is influenced by both,
402 maritime and continental air masses. The latter can lead to strong surface inversions above
403 the Mauritanian Upwelling and strongly suppressed mixing of surface air. Although our
404 investigations revealed low MABL heights close to the Peruvian coast, the distinct surface
405 inversions as observed above the Mauritanian Upwelling are not present in the available
406 radiosonde data for this Peruvian Upwelling region. In addition, the relatively low sea-air
407 fluxes of bromoform and dibromomethane, caused by moderate winds and small
408 concentration gradients between the surface ocean and the surface atmosphere, as well as the
409 short lifetime of methyl iodide lead to an insufficient enrichment of VSLs in the atmosphere.
410 The observed air masses therefore contain VSLs mixing ratios which are predominantly
411 advected. This is confirmed by our computed ADR (Section 3.4). The backward trajectories
412 reveal air masses originating from the open ocean, which are transported along the coast for
413 about 5 days until they reach the ship. In combination with the distinct trade inversion acting
414 as strong barrier to the vertical mixing of trace gases, air-masses along the coast travel close
415 to the surface where they can be enriched with local emissions before they are observed on-
416 board. In addition, the in-situ observed oceanic emissions along the cruise track of R/V
417 METEOR therefore cause small variations to the accumulated background mixing ratios of
418 the advected air masses. This leads to lower correlation coefficients between the MABL
419 height and the VSLs abundances compared to the Mauritanian Upwelling.
420 Although the oceanic emissions are already well mixed within days below the trade
421 inversion, methyl iodide mixing ratios indicate a positive correlation with the trade inversion
422 height, which is unexpected. The correlation coefficient might be artificial, as we observe
423 elevated methyl iodide above the upwelling, where trade wind inversion heights are missing
424 but can be assumed to be low (Riehl, 1954), which is also indicated by the correlation

425 coefficients with SAT and SST. Nevertheless, this circumstance should be taken into account
426 in future studies.

427 The contribution of oceanic emissions to the atmospheric mixing ratios in the MABL of the
428 Peruvian upwelling reveals to be rather low in its more open ocean area under the given
429 meteorological conditions. While the cruise track covered a representative area of the
430 Peruvian upwelling elevated oceanic VSLs emissions that could explain the generally high
431 atmospheric VSLs were only observed for methyl iodide. Bromocarbon emissions would
432 have to be two magnitudes larger to explain the observed VMR in the more open ocean
433 regions and a magnitude larger in the direct coastal upwelling regions with low MABL
434 heights. These observations of the brominated compounds need to include upwind advection
435 of elevated sources from the South, and higher elevated coastal emissions not measured
436 during the cruise, while dynamical fluctuations in emissions scenarios close to the cruise time
437 and place may also have to be considered.

438 Uncertainties may result from the applied method, which accounts for a 400 m² box around a
439 measurement point assuming steady state. The cruise track covered a significantly large area
440 of the Peruvian Upwelling between 5° S and 16° S and higher elevated seas surface
441 concentrations and emissions are not to be expected during these rather stable meteorological
442 conditions. Additional uncertainties in our source-loss estimate may arise from deficiencies in
443 the meteorological input fields from ERA-Interim reanalysis as well as from the air mass
444 transport simulated by FLEXPART. Both could lead to either a shorter or longer residence
445 time of the surface air masses within the MABL or below the trade inversion and thus
446 influence the COL term. In particular very close to the coast, where the source-loss estimate
447 could not be applied due to the trajectory analysis gaps (Section 2.5), the ODRs of the
448 compounds might be different. Here potential high coastal emissions in combination with
449 stable atmospheric stratification leading to slow vertical transport into the free troposphere,
450 could significantly increase the oceanic contribution to the MABL and to the atmosphere
451 below the trade inversion and explain the elevated atmospheric mixing ratios. In addition,
452 different parameterizations for the wind-based transfer coefficient k_w , as discussed in
453 Lennartz et al. (2015) and Fuhlbrügge et al (2015) in more detail, can impact the air-sea gas
454 exchange and thus the ODRs. Applying the k_w parameterizations of Liss and Merlivat
455 (1986) as well as Wanninkhof and McGillis (1999) lead both to mean ODRs in the MABL of
456 0.02 (bromoform), 0.07 (dibromomethane) and 0.21 (methyl iodide) and below the trade
457 inversion of 0.08 / 0.08 (bromoform), 0.25 / 0.26 (dibromomethane) and 0.69 / 0.75 (methyl
458 iodide) and thus an even lower oceanic contribution to the atmosphere in this region. Further

459 uncertainties may arise from variations of the MABL VSLs lifetimes and thus the chemical
460 degradation of the compounds we use in this study. This would affect the computed
461 advection (ADR) and not the oceanic contribution. After the air masses are observed on R/V
462 METEOR, the 10 day FLEXPART forward trajectories reveal a near-surface transport
463 towards the equator (Figure 2c-d). These trajectories predominantly stay below 1 km altitude
464 due to the horizontal extent of the trade inversion. The contribution of oceanic VSLs
465 emissions from the Peruvian Upwelling to the free troposphere above this region is therefore
466 strongly suppressed by the trade inversion (Figure 4d). A contribution of oceanic emissions
467 from the Peruvian Upwelling to the free troposphere is only achieved in the inner tropics after
468 a transport time of 5 – 8 days, where the VSLs abundances are transported into higher
469 altitudes. Since the lifetime of methyl iodide is only 4 days in the MABL a significant
470 contribution of methyl iodide from the Peruvian upwelling to observations made by
471 Yokouchi et al. (2008) at San Cristobal, Galapagos is not to be expected. However, it can
472 partly explain the elevated IO observed above the Peruvian upwelling (Hepach et al., 2016, to
473 be submitted; Schönhardt et al., 2008). The elevated mixing ratios of methyl iodide is further
474 investigated by Hepach et al. (2015b). It has to be noted that the determined low contribution
475 of oceanic emissions and boundary layer air to the free troposphere in this region is only
476 representative for normal El Niño Southern Oscillation conditions as it was observed in
477 December 2012
478 ([http://www.cpc.ncep.noaa.gov/products/analysis_monitoring/enso_disc_nov2012/ensodisc.p](http://www.cpc.ncep.noaa.gov/products/analysis_monitoring/enso_disc_nov2012/ensodisc.pdf)
479 [df](http://www.cpc.ncep.noaa.gov/products/analysis_monitoring/enso_disc_nov2012/ensodisc.pdf)). Since the Walker Circulation is reversed during El Niño, upwelling along the Peruvian
480 coast is known to be suppressed and convective activity enhanced (Philander, 1989).

481

482 **5. Summary**

483 This study investigated the contribution of oceanic emissions to VSLs abundances in the
484 lowermost atmosphere as well as meteorological constraints on this contribution above both,
485 coastal upwelling and open ocean along the Peruvian coast during December 2012.
486 Meteorological data were obtained on R/V METEOR near the ocean surface and by
487 radiosondes up to the stratosphere. Oceanic VSLs emissions along the cruise track were
488 determined from air and surface water data. The transport of air masses was determined with
489 FLEXPART trajectories.

490 Oceanic upwelling was observed close to the Peruvian coast. On average a low, stable MABL
491 height of 307 ± 177 m was encountered during the cruise, decreasing to on average 100 m
492 above the upwelling. A distinct trade inversion at 1.1 ± 0.3 km height evolved as the

493 dominant transport barrier for MABL air into the free troposphere during the cruise. The
494 halogenated VSLS bromoform and dibromomethane showed low oceanic emissions of $117 \pm$
495 $492 \text{ pmol m}^{-2} \text{ hr}^{-1}$ for bromoform and $245 \pm 299 \text{ pmol m}^{-2} \text{ hr}^{-1}$ for dibromomethane, while
496 methyl iodide emissions were elevated with $856 \pm 623 \text{ pmol m}^{-2} \text{ hr}^{-1}$. The atmospheric
497 mixing ratios of the compounds were elevated with 2.9 ± 0.7 ppt (bromoform), 1.3 ± 0.3 ppt
498 (dibromomethane) and 1.5 ± 0.5 ppt (methyl iodide). The oceanic emissions along the cruise
499 track explained on average only 3 % (-8 to 33 %) of bromoform, 10 % (-5 to 45 %) of
500 dibromomethane, and 28 % (3 to 80 %) of methyl iodide abundances in the MABL. Thus, the
501 expected significant contribution of local oceanic VSLS emissions from the Peruvian
502 upwelling to the overlying atmosphere was not captured during the time and location of the
503 cruise. The elevated atmospheric VSLS mixing ratios above the Peruvian upwelling therefore
504 appear largely advected and enriched along the Peruvian coast before reaching the ship.
505 Additional potential source regions must exist closer to the coast and also further South of the
506 cruise track along the coast line. Nevertheless, significant correlations between the MABL
507 height and marine atmospheric abundances of the VSLS reveal an impact of the oceanic
508 emissions on the atmospheric VSLS mixing ratio variations.

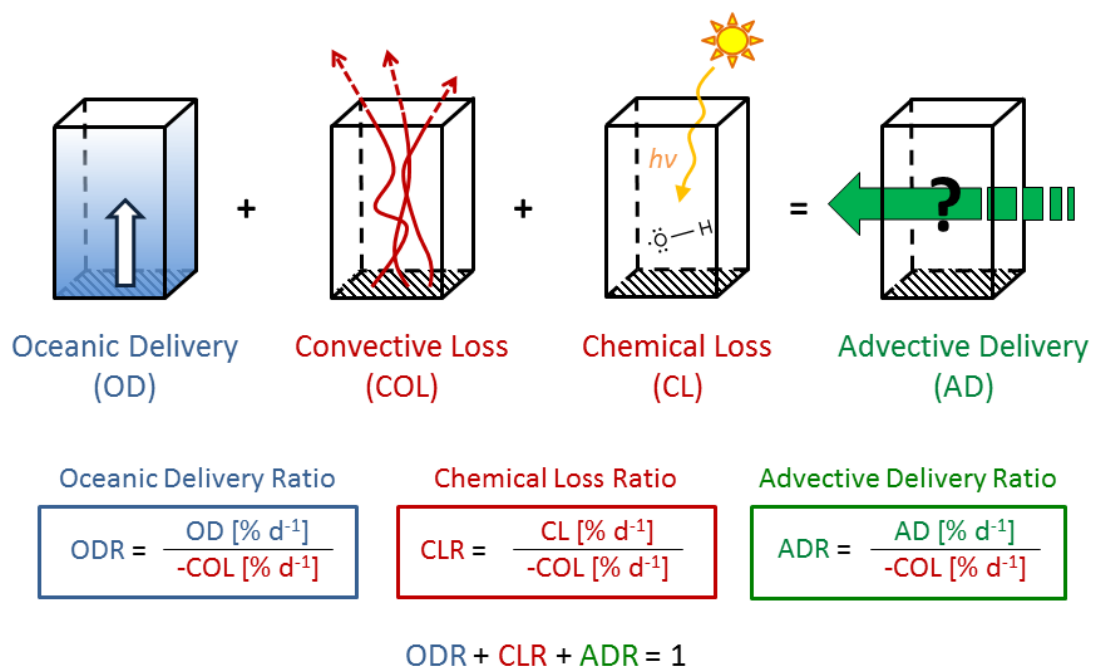
509 Our study confirms that MABL height and stability are generally related with atmospheric
510 VSLS abundances above oceanic upwelling regions. Additionally, a widespread trade
511 inversion can lead to a near-surface accumulation of the VSLS and thus also impact oceanic
512 emissions. Despite the observed elevated atmospheric concentrations during the cruise, a
513 significant contribution of oceanic emissions to the atmosphere, in particular of the
514 bromocarbons bromoform and dibromomethane, was not identified in the observed area
515 during the time of the cruise. Further studies are necessary to clearly uncover the source
516 regions of the elevated atmospheric VSLS in the Peruvian upwelling. Also the double
517 transport barrier phenomena should be investigated in future studies of other oceanic
518 upwelling regions as well.

519

520 **Acknowledgements**

521 This study was supported by the BMBF grant SOPRAN II FKZ 03F0611A. We acknowledge
522 the authorities of Peru for the permissions to work in their territorial waters. We thank the
523 European Centre for medium range weather forecast (ECMWF) for the provision of ERA-
524 Interim reanalysis data and the Lagrangian particle dispersion model FLEXPART used in this
525 publication. We also like to thank the captain and crew of R/V METEOR, and the Deutscher
526 Wetterdienst (DWD) for the support.

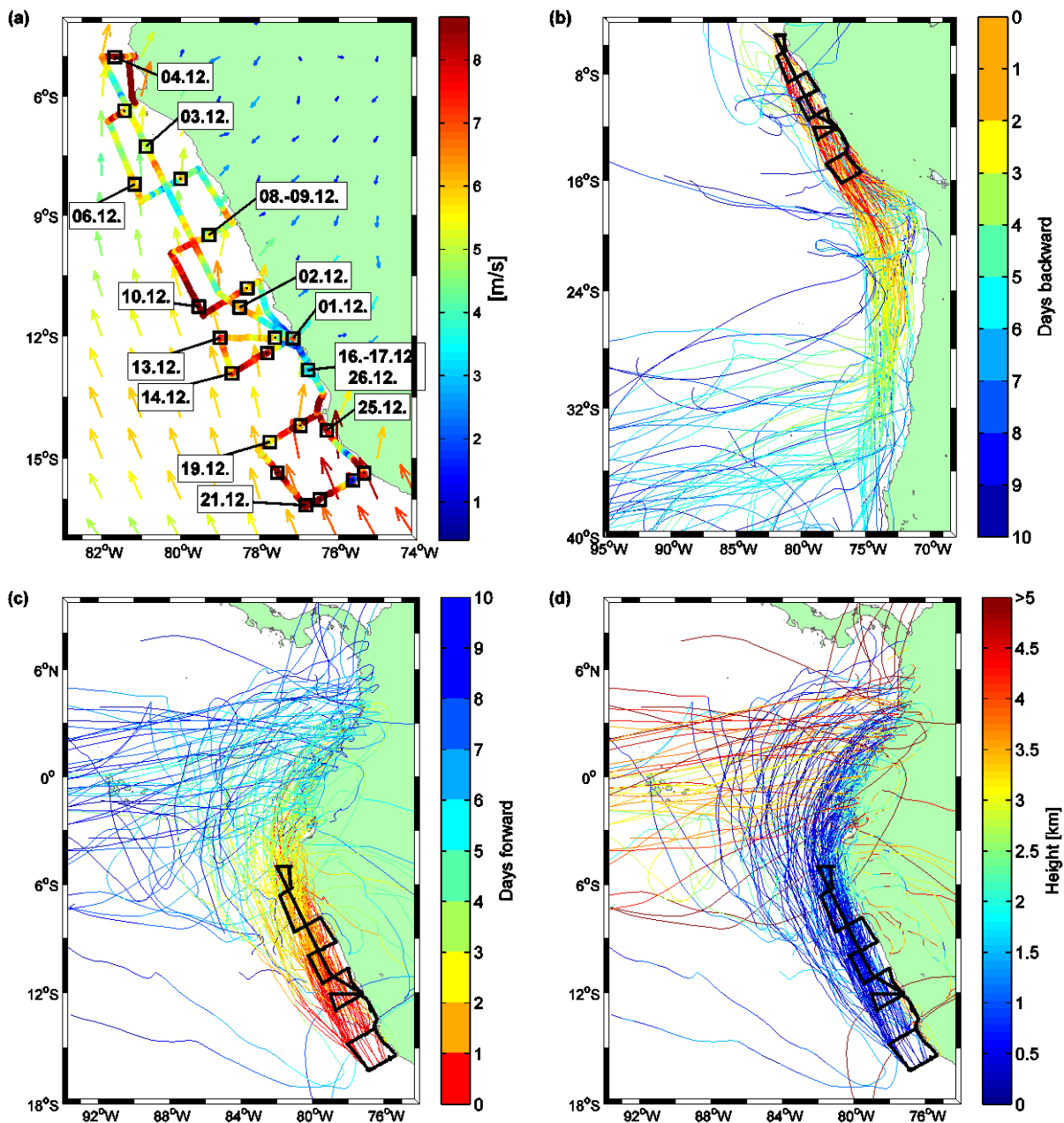
527



529

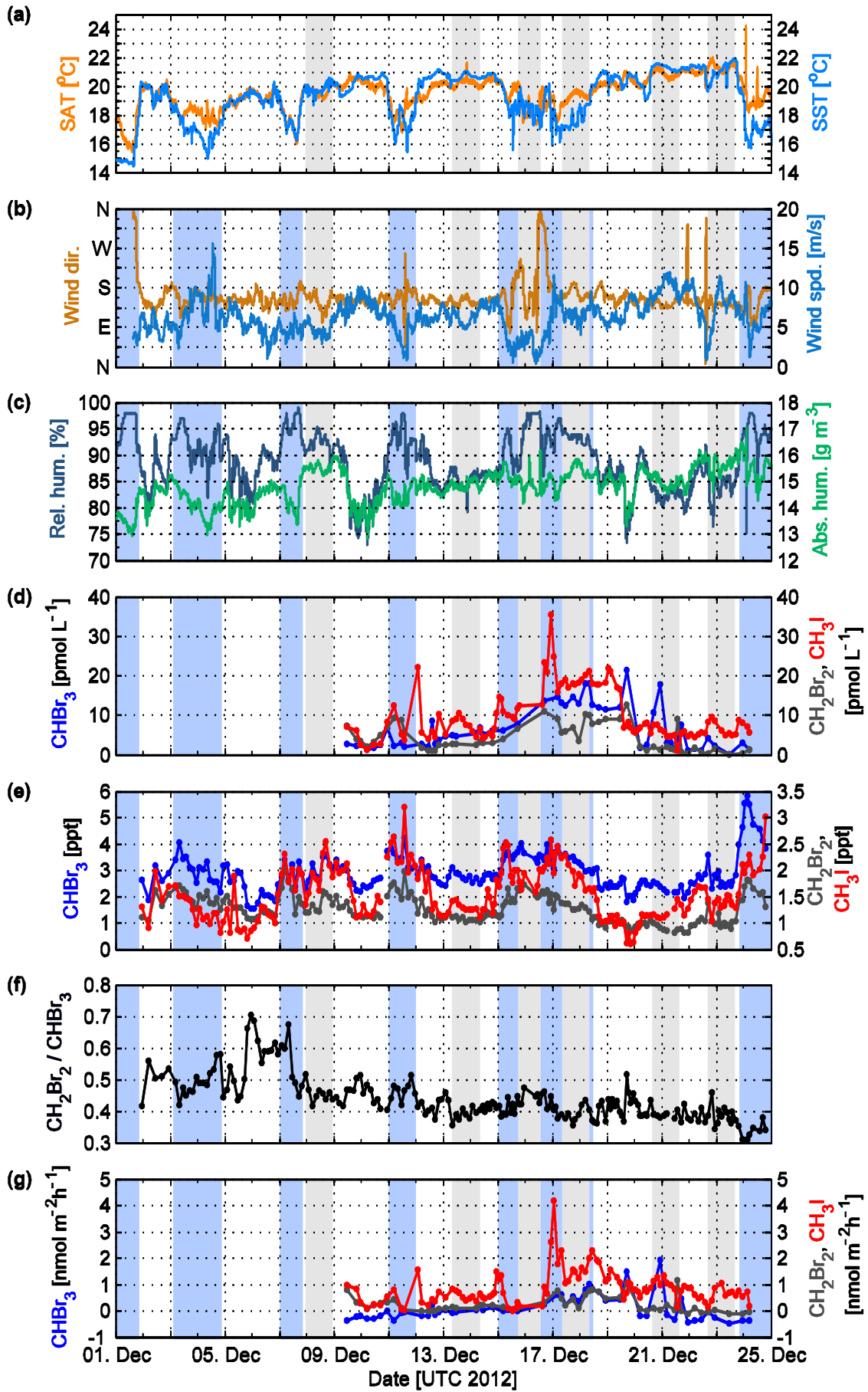
530 Figure 1: Schematic summary of the components of the applied mass-balance concept from
 531 Fuhlbrügge et al. (2015): Oceanic Delivery (OD), the Convective Loss (COL), the Chemical
 532 Loss (CL), the Advective Delivery (AD), the Oceanic Delivery Ratio (ODR), the Chemical
 533 Loss Ratio (CLR) and the Advective Delivery Ratio (ADR). The shaded area reflects an area
 534 of 400 m².

535



536

537 Figure 2a-d: (a) 10 minute mean of wind speed observed on R/V METEOR displayed along
 538 the cruise track; monthly mean (December 2012) of 10 m wind speed and direction from
 539 ERA-Interim displayed as arrows. (b) Extract from 10-day FLEXPART backward trajectories
 540 coloured according to the time until they reach the specific ship position on the cruise track of
 541 R/V METEOR (black). (c) Extract from 10-day FLEXPART forward trajectories coloured
 542 according to the time since they were released. (d) same as c) coloured according to the
 543 height (km) of the trajectories.

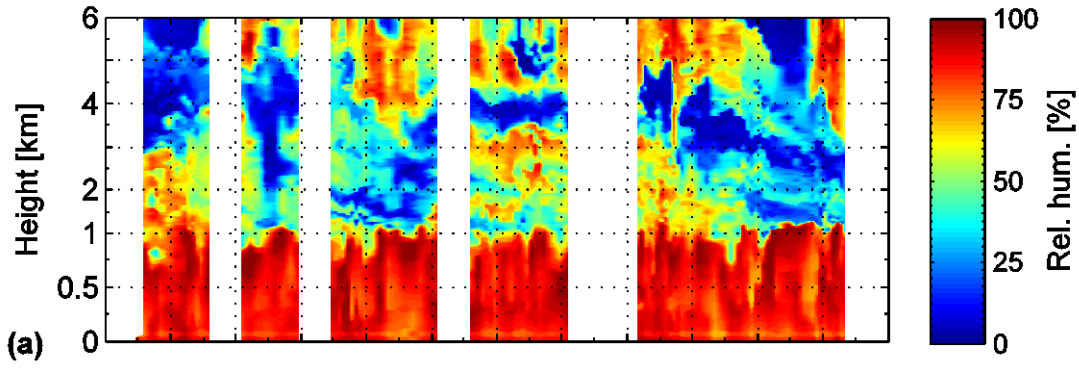


545 Figure 3a-e: Observations during December 1 – 25, 2012 on R/V METEOR. Diurnal stations
546 are indicated by grey background shades. (a) 10 minute mean of the SAT (orange) and the
547 SST (blue) in °C. According to SST decrease, upwelling regions are marked with a light blue
548 background shade in Figure 3b-e. (b) 10 minute mean of wind direction in cardinal directions
549 (ocher) and wind speed in m/s (blue). (c) 10 minute mean of relative humidity in % (dark
550 blue) and absolute humidity in gm^{-3} (green). (d) Oceanic surface concentrations of
551 bromoform (CHBr_3 , blue), dibromomethane (CH_2Br_2 , dark grey) and methyl iodide (CH_3I ,
552 red) in pmol L^{-1} . (e) Atmospheric mixing ratios of bromoform, dibromomethane and methyl
553 iodide in ppt. (f) Concentration ratio of dibromomethane and bromoform. (g) Sea-air flux for
554 bromoform, dibromomethane and methyl iodide in $\text{pmol m}^{-2} \text{h}^{-1}$.

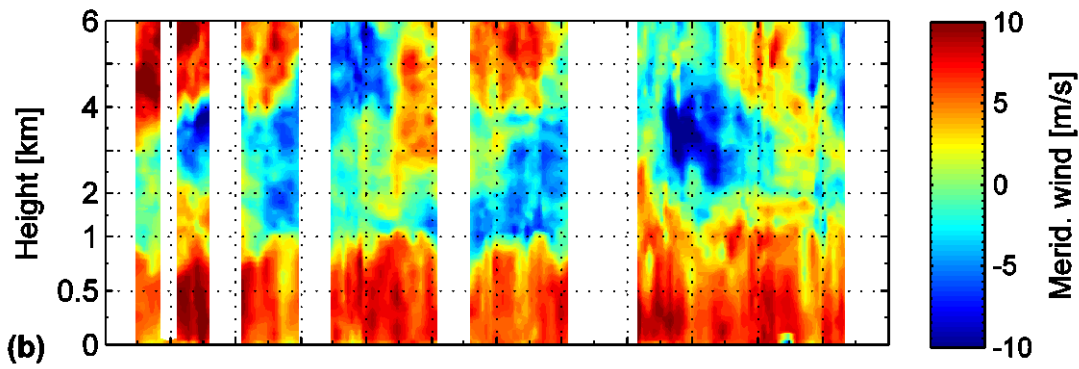
555 Table 1: Oceanic concentrations, atmospheric mixing ratios and sea-air fluxes of bromoform
 556 (CHBr_3), dibromomethane (CH_2Br_2), the concentration ratio of bromoform and
 557 dibromomethane and methyl iodide (CH_3I) observed during the cruise. Values are given in
 558 mean $\pm 1\sigma$ [range].

	CHBr_3	CH_2Br_2	$\text{CH}_2\text{Br}_2 / \text{CHBr}_3$	CH_3I
Oceanic concentration [pmol L^{-1}]	6.6 ± 5.5 [0.2 – 21.5]	4.3 ± 3.4 [0.2 – 12.7]	0.9 ± 0.8 [0.1 – 4.2]	9.8 ± 6.3 [1.1 – 35.4]
Atmospheric mixing ratio [ppt]	2.9 ± 0.7 [1.5 – 5.9]	1.3 ± 0.3 [0.8 – 2.0]	0.4 ± 0.1 [0.3 – 0.7]	1.5 ± 0.5 [0.6 – 3.2]
Sea-air flux [$\text{pmol m}^{-2} \text{hr}^{-1}$]	117 ± 492 [-477 – 1916]	245 ± 299 [-112 – 1169]	0.4 ± 8.6 [-24.5 – 48.9]	856 ± 623 [18 - 4179]

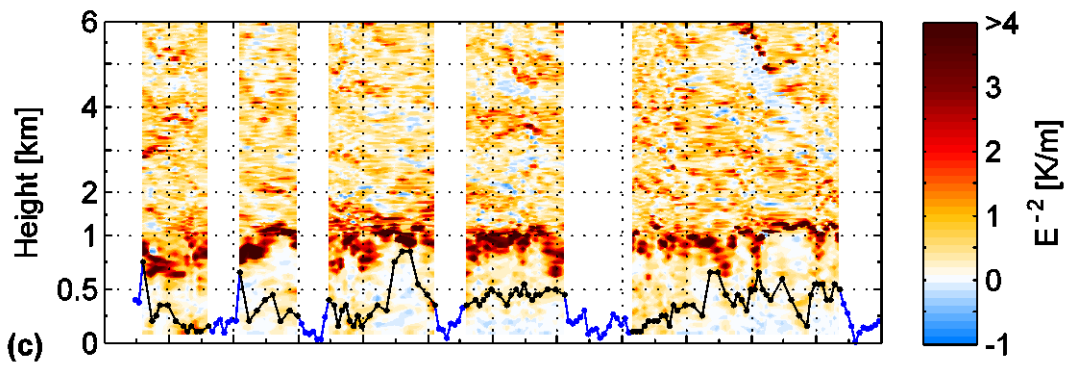
559



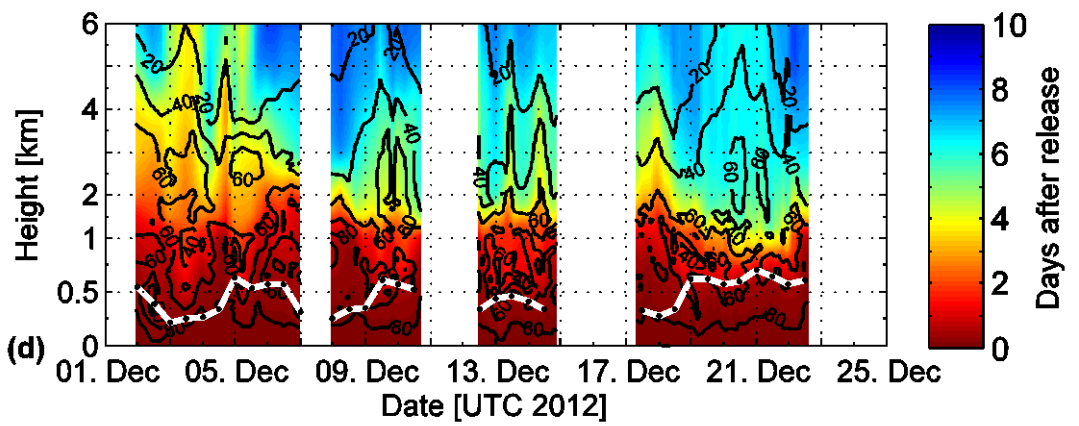
560



561



562



563

564 Figure 4: (a-c) Radiosonde observations of the lower 6 km of the atmosphere between
565 December 2 and 24, 2012 on R/V Meteor. Shown are (a) the relative humidity in %, (b) the
566 meridional wind in m/s and (c) the gradient of the virtual potential temperature in E^{-2} K/m in
567 combination with the determined MABL height (black) and the complimented MABL height
568 above the oceanic upwelling from the multiple linear regressions (blue). (d) Distribution of
569 10-day FLEXPART forward trajectories. The black contour lines give the amount of
570 trajectories in percentage that reach a specific altitude within the 10 days. The elapsed time in
571 days until these trajectories reach this height is reflected by the colour shading. The white line
572 shows the ERA-Interim MABL height at the ship position. Trajectory analyses gaps close to
573 the coast are whitened (Section 2.5). The y-axes are non-linear.

574 Table 2: Mean $\pm 1\sigma$ of Oceanic Delivery (OD), Advective Delivery (AD), Chemical Loss
 575 (CL), Convective Loss (COL), Oceanic Delivery Ratio (ODR), Advective Delivery Ratio
 576 (ADR) and Chemical Loss Ratio (CLR) of bromoform (CHBr_3), dibromomethane (CH_2Br_2)
 577 and methyl iodide (CH_3I). Parameters have been computed for a box with the vertical
 578 extension of the MABL height (MABLH) and a mean trade inversion height of 1.1 km (TIH).

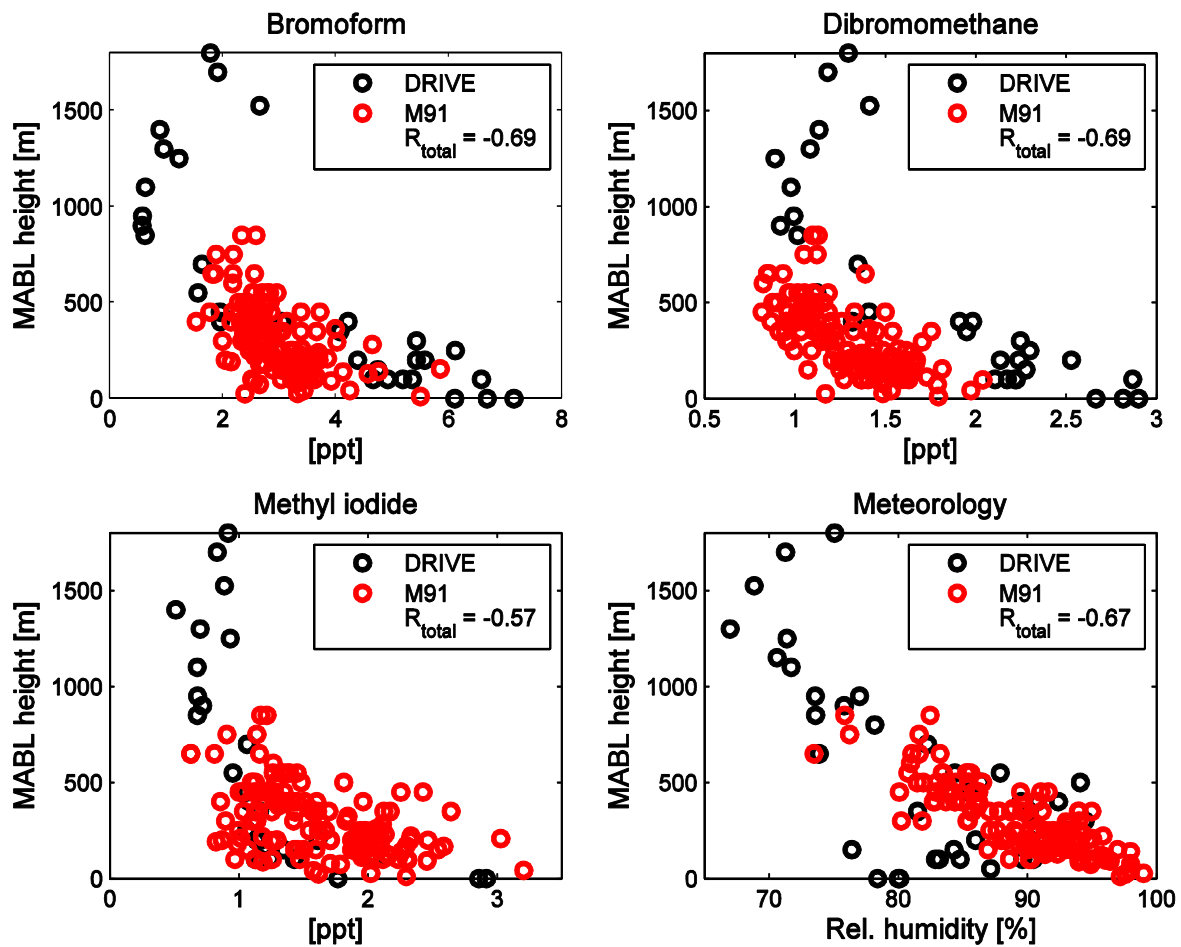
		OD [% d ⁻¹]	AD [% d ⁻¹]	CL [% d ⁻¹]	COL [% d ⁻¹]	ODR	ADR	CLR
CHBr_3	MABLH	9.1 ± 28.0	349.0 ± 113.4	-7.1	-351.0 ± 109.4	0.03 ± 0.08	0.99 ± 0.08	-0.02 ± 0.01
	TIH	3.9 ± 12.0	53.2 ± 23.2	-7.1	-50.0 ± 18.4	0.11 ± 0.4	1.06 ± 0.39	-0.17 ± 0.07
CH_2Br_2	MABLH	32.1 ± 38.7	320.1 ± 115.6	-1.2	-351.0 ± 109.4	0.10 ± 0.11	0.90 ± 0.11	-0.00 ± 0.00
	TIH	13.8 ± 16.5	37.4 ± 25.9	-1.2	-50.0 ± 18.4	0.33 ± 0.54	0.7 ± 0.54	-0.03 ± 0.01
CH_3I	MABLH	88.9 ± 48.1	286.1 ± 119.7	-24.0	-351.0 ± 109.4	0.28 ± 0.17	0.80 ± 0.16	-0.08 ± 0.03
	TIH	36.8 ± 20.5	37.2 ± 32.1	-24.0	-50.0 ± 18.4	0.92 ± 0.69	0.64 ± 0.55	-0.56 ± 0.24

579

580 Table 3: Spearman correlation coefficients (R) of meteorological parameters, MABL height
 581 and trade inversion height correlated with atmospheric bromoform (CHBr₃), dibromomethane
 582 (CH₂Br₂) and methyl iodide (CH₃I). MABL height* is the determined MABL height from the
 583 radiosonde launches, complimented by the regressed MABL height (Section 3.3). Bold
 584 coefficients have a p-value of < 0.05.

	MABL height	MABL height*	Trade inversion	CHBr ₃	CH ₂ Br ₂	CH ₃ I
Wind speed	0.35	0.44	-0.06	-0.38	-0.53	-0.33
SAT	0.65	0.79	0.24	-0.50	-0.78	-0.37
SST	0.66	0.80	0.23	-0.57	-0.81	-0.42
SAT – SST	-0.39	-0.47	-0.11	0.38	0.48	0.30
Rel. humidity	-0.77	-0.81	-0.06	0.74	0.77	0.67
MABL height*	-	-	0.08	-0.55	-0.61	-0.45
CHBr ₃	-0.55	-0.60	-0.03	-	0.79	0.79
CH ₂ Br ₂	-0.61	-0.72	-0.02	0.79	-	0.66
CH ₃ I	-0.45	-0.50	0.30	0.79	0.66	-

585



586

587 Figure 5: Scatter plots of atmospheric mixing ratios of bromoform, dibromomethane, methyl
 588 iodide and relative humidity vs. MABL height. Black circles reflect observations from the
 589 DRIVE campaign in the Mauritanian Upwelling (Fuhlbrügge et al., 2013) and red circles
 590 from this study (M91). R_{total} gives the Spearman correlation coefficients for both data sets
 591 together.

592

593 **References**

- 594 Butler, J., King, D., Lobert, J., Montzka, S., Yvon-Lewis, S., Hall, B., Warwick, N., Mondeel, D., Aydin,
595 M., and Elkins, J.: Oceanic distributions and emissions of short-lived halocarbons, *Global*
596 *Biogeochemical Cycles*, 21, 10.1029/2006GB002732, 2007.
- 597 Carpenter, L., Liss, P., and Penkett, S.: Marine organohalogens in the atmosphere over the Atlantic
598 and Southern Oceans, *Journal of Geophysical Research-Atmospheres*, 108, 10.1029/2002JD002769,
599 2003.
- 600 Carpenter, L., Jones, C., Dunk, R., Hornsby, K., and Woeltjen, J.: Air-sea fluxes of biogenic bromine
601 from the tropical and North Atlantic Ocean, *Atmospheric Chemistry and Physics*, 9, 1805-1816, 2009.
- 602 Carpenter, L., Fleming, Z., Read, K., Lee, J., Moller, S., Hopkins, J., Purvis, R., Lewis, A., Muller, K.,
603 Heinold, B., Herrmann, H., Fomba, K., van Pinxteren, D., Muller, C., Tegen, I., Wiedensohler, A.,
604 Muller, T., Niedermeier, N., Achterberg, E., Patey, M., Kozlova, E., Heimann, M., Heard, D., Plane, J.,
605 Mahajan, A., Oetjen, H., Ingham, T., Stone, D., Whalley, L., Evans, M., Pilling, M., Leigh, R., Monks, P.,
606 Karunaharan, A., Vaughan, S., Arnold, S., Tschirner, J., Pohler, D., Friess, U., Holla, R., Mendes, L.,
607 Lopez, H., Faria, B., Manning, A., and Wallace, D.: Seasonal characteristics of tropical marine
608 boundary layer air measured at the Cape Verde Atmospheric Observatory, *Journal of Atmospheric*
609 *Chemistry*, 67, 87-140, 10.1007/s10874-011-9206-1, 2010.
- 610 Carpenter, L. J., Reimann, S., Burkholder, J. B., Clerbaux, C., Hall, B. D., Hossaini, R., Laube, J. C., and
611 Yvon-Lewis, S. A.: Update on Ozone-Depleting Substances (ODSs) and Other Gases of Interest to the
612 Montreal Protocol, in: *Scientific Assessment of Ozone Depletion: 2014*, edited by: Engel, A., and
613 Montzka, S. A., World Meteorological Organization, Geneva, 2014.
- 614 Codispoti, L. A., Dugdale, R. C., and Minas, H. J.: A comparison of the nutrient regimes off Northwest
615 Africa, Peru and Baja California, *Rapport et Procés-verbaux des réunions. Conseil permanent*
616 *International pour l'Exploration de la Mer*, 184-201 pp., 1982.
- 617 Dix, B., Baidara, S., Bresch, J., Hall, S., Schmidt, K., Wang, S., and Volkamer, R.: Detection of iodine
618 monoxide in the tropical free troposphere, *Proceedings of the National Academy of Sciences of the*
619 *United States of America*, 110, 2035-2040, 10.1073/pnas.1212386110, 2013.
- 620 Forster, C., Stohl, A., and Seibert, P.: Parameterization of convective transport in a Lagrangian
621 particle dispersion model and its evaluation, *Journal of Applied Meteorology and Climatology*, 46,
622 403-422, 10.1175/JAM2470.1, 2007.
- 623 Fuhlbrügge, S., Krüger, K., Quack, B., Atlas, E., Hepach, H., and Ziska, F.: Impact of the marine
624 atmospheric boundary layer conditions on VSLs abundances in the eastern tropical and subtropical
625 North Atlantic Ocean, *Atmospheric Chemistry and Physics*, 13, 6345-6357, 10.5194/acp-13-6345-
626 2013, 2013.
- 627 Fuhlbrügge, S., Quack, B., Tegtmeier, S., Atlas, E., Hepach, H., Shi, Q., Raimund, S., and Krüger, K.:
628 The contribution of oceanic very short lived halocarbons to marine and free troposphere air over the
629 tropical West Pacific, *Atmos. Chem. Phys. Discuss.*, 15, 17887-17943, 10.5194/acpd-15-17887-2015,
630 2015.
- 631 Garreaud, R., and Munoz, R.: The low-level jet off the west coast of subtropical South America:
632 Structure and variability, *Monthly Weather Review*, 133, 2246-2261, 10.1175/MWR2972.1, 2005.
- 633 Gómez Martin, J., Mahajan, A., Hay, T., Prados-Roman, C., Ordonez, C., MacDonald, S., Plane, J.,
634 Sorribas, M., Gil, M., Mora, J., Reyes, M., Oram, D., Leedham, E., and Saiz-Lopez, A.: Iodine chemistry
635 in the eastern Pacific marine boundary layer, *Journal of Geophysical Research-Atmospheres*, 118,
636 887-904, 10.1002/jgrd.50132, 2013.
- 637 Hepach, H., Quack, B., Ziska, F., Fuhlbrügge, S., Atlas, E., Krüger, K., Peeken, I., and Wallace, D. W. R.:
638 Drivers of diel and regional variations of halocarbon emissions from the tropical North East Atlantic,
639 *Atmos. Chem. Phys.*, 14, 10.5194/acp-14-1255-2014, 2014.
- 640 Hepach, H., Quack, B., Raimund, S., Fischer, T., Atlas, E. L., and Bracher, A.: Halocarbon emissions
641 and sources in the equatorial Atlantic Cold Tongue, *Biogeosciences Discuss.*, 12, 5559-5608,
642 10.5194/bgd-12-5559-2015, 2015a.

643 Hepach, H., Quack, B., Tegtmeier, S., Engel, A., Bracher, A., Fuhlbrügge, S., Raimund, S., Lampel, J., L.,
644 G., and Krüger, K.: Contributions of biogenic halogenated compounds from the Peruvian upwelling
645 to the tropical troposphere, to be submitted, 2015b.

646 Hepach, H., Quack, B., Tegtmeier, S., Engel, A., Bracher, A., Fuhlbrügge, S., L., G., Atlas, E., Lampel, J.,
647 Frieß, U., and Krüger, K.: Biogenic halocarbons from the Peruvian upwelling region as tropospheric
648 halogen source, to be submitted, 2016.

649 Hossaini, R., Chipperfield, M., Monge-Sanz, B., Richards, N., Atlas, E., and Blake, D.: Bromoform and
650 dibromomethane in the tropics: a 3-D model study of chemistry and transport, *Atmospheric*
651 *Chemistry and Physics*, 10, 719-735, 10.5194/acp-10-719-2010, 2010.

652 Höflich, O.: The meteorological effects of cold upwelling water areas, *Geoforum*, 3, 35-46,
653 10.1016/0016-7185(72)90084-X, 1972.

654 Lennartz, S. T., Krysztofiak, G., Marandino, C. A., Sinnhuber, B. M., Tegtmeier, S., Ziska, F., Hossaini,
655 R., Krüger, K., Montzka, S. A., Atlas, E., Oram, D. E., Keber, T., Bönisch, H., and Quack, B.: Modelling
656 marine emissions and atmospheric distributions of halocarbons and dimethyl sulfide: the influence
657 of prescribed water concentration vs. prescribed emissions, *Atmos. Chem. Phys.*, 15, 11753-11772,
658 10.5194/acp-15-11753-2015, 2015.

659 Liss, P. S., and Merlivat, L.: Air-Sea Gas Exchange Rates: Introduction and Synthesis, in: *The Role of*
660 *Air-Sea Exchange in Geochemical Cycling*, edited by: Buat-Menard, P., Reidel, D., and Norwell, M.,
661 Springer Netherlands, 113-127, 1986.

662 Liu, Y., Yvon-Lewis, S., Thornton, D., Butler, J., Bianchi, T., Campbell, L., Hu, L., and Smith, R.: Spatial
663 and temporal distributions of bromoform and dibromomethane in the Atlantic Ocean and their
664 relationship with photosynthetic biomass, *Journal of Geophysical Research-Oceans*, 118, 3950-3965,
665 10.1002/jgrc.20299, 2013.

666 Mahajan, A., Martin, J., Hay, T., Royer, S., Yvon-Lewis, S., Liu, Y., Hu, L., Prados-Roman, C., Ordonez,
667 C., Plane, J., and Saiz-Lopez, A.: Latitudinal distribution of reactive iodine in the Eastern Pacific and its
668 link to open ocean sources, *Atmospheric Chemistry and Physics*, 12, 11609-11617, 10.5194/acp-12-
669 11609-2012, 2012.

670 McGivern, W., Sorkhabi, O., Suits, A., Derecskei-Kovacs, A., and North, S.: Primary and secondary
671 processes in the photodissociation of CHBr₃, *Journal of Physical Chemistry a*, 104, 10085-10091,
672 10.1021/jp0005017, 2000.

673 Nightingale, P., Malin, G., Law, C., Watson, A., Liss, P., Liddicoat, M., Boutin, J., and Upstill-Goddard,
674 R.: In situ evaluation of air-sea gas exchange parameterizations using novel conservative and volatile
675 tracers, *Global Biogeochemical Cycles*, 14, 373-387, 10.1029/1999GB900091, 2000.

676 O'Brien, L., Harris, N., Robinson, A., Gostlow, B., Warwick, N., Yang, X., and Pyle, J.: Bromocarbons in
677 the tropical marine boundary layer at the Cape Verde Observatory - measurements and modelling,
678 *Atmospheric Chemistry and Physics*, 9, 9083-9099, 10.5194/acp-9-9083-2009, 2009.

679 Philander, G.: El-Nino and La-Nina, *American Scientist*, 77, 451-459, 1989.

680 Quack, B., Atlas, E., Petrick, G., Stroud, V., Schauffler, S., and Wallace, D.: Oceanic bromoform
681 sources for the tropical atmosphere, *Geophysical Research Letters*, 31, 10.1029/2004GL020597,
682 2004.

683 Quack, B., Atlas, E., Petrick, G., and Wallace, D.: Bromoform and dibromomethane above the
684 Mauritanian upwelling: Atmospheric distributions and oceanic emissions, *Journal of Geophysical*
685 *Research-Atmospheres*, 112, 10.1029/2006JD007614, 2007.

686 Raimund, S., Quack, B., Bozec, Y., Vernet, M., Rossi, V., Garcon, V., Morel, Y., and Morin, P.: Sources
687 of short-lived bromocarbons in the Iberian upwelling system, *Biogeosciences*, 8, 1551-1564,
688 10.5194/bg-8-1551-2011, 2011.

689 Rasmussen, R., Khalil, M., Gunawardena, R., and Hoyt, S.: Atmospheric methyl-iodide (CH₃I), *Journal*
690 *of Geophysical Research-Oceans and Atmospheres*, 87, 3086-3090, 10.1029/JC087iC04p03086,
691 1982.

692 Riehl, H.: *Tropical meteorology*, McGraw-Hill, New York-London, 1954.

693 Riehl, H.: *Climate and Weather in the Tropics*, Academic Press, London, 1979.

694 Saiz-Lopez, A., Lamarque, J., Kinnison, D., Tilmes, S., Ordonez, C., Orlando, J., Conley, A., Plane, J.,
695 Mahajan, A., Santos, G., Atlas, E., Blake, D., Sander, S., Schauffler, S., Thompson, A., and Brasseur, G.:
696 Estimating the climate significance of halogen-driven ozone loss in the tropical marine troposphere,
697 *Atmospheric Chemistry and Physics*, 12, 3939-3949, 10.5194/acp-12-3939-2012, 2012.
698 Saiz-Lopez, A., and von Glasow, R.: Reactive halogen chemistry in the troposphere, *Chemical Society*
699 *Reviews*, 41, 6448-6472, 10.1039/c2cs35208g, 2012.
700 Schauffler, S., Atlas, E., Blake, D., Flocke, F., Lueb, R., Lee-Taylor, J., Stroud, V., and Travnicek, W.:
701 Distributions of brominated organic compounds in the troposphere and lower stratosphere, *Journal*
702 *of Geophysical Research-Atmospheres*, 104, 21513-21535, 10.1029/1999JD900197, 1999.
703 Schönhardt, A., Richter, A., Wittrock, F., Kirk, H., Oetjen, H., Roscoe, H., and Burrows, J.:
704 Observations of iodine monoxide columns from satellite, *Atmospheric Chemistry and Physics*, 8, 637-
705 653, 10.5194/acp-8-637-2008, 2008.
706 Seibert, P., Beyrich, F., Gryning, S., Joffre, S., Rasmussen, A., and Tercier, P.: Review and
707 intercomparison of operational methods for the determination of the mixing height, *Atmospheric*
708 *Environment*, 34, 1001-1027, 10.1016/S1352-2310(99)00349-0, 2000.
709 Simpson, W., Brown, S., Saiz-Lopez, A., Thornton, J., and von Glasow, R.: Tropospheric Halogen
710 Chemistry: Sources, Cycling, and Impacts, *Chemical Reviews Article ASAP*, 4035-4062,
711 10.1021/cr5006638, 2015.
712 Stohl, A., Hittenberger, M., and Wotawa, G.: Validation of the Lagrangian particle dispersion model
713 FLEXPART against large-scale tracer experiment data, *Atmospheric Environment*, 32, 4245-4264,
714 10.1016/S1352-2310(98)00184-8, 1998.
715 Stohl, A., and Thomson, D.: A density correction for Lagrangian particle dispersion models,
716 *Boundary-Layer Meteorology*, 90, 155-167, 10.1023/A:1001741110696, 1999.
717 Stohl, A., and Trickl, T.: A textbook example of long-range transport: Simultaneous observation of
718 ozone maxima of stratospheric and North American origin in the free troposphere over Europe,
719 *Journal of Geophysical Research-Atmospheres*, 104, 30445-30462, 10.1029/1999JD900803, 1999.
720 Stohl, A., Forster, C., Frank, A., Seibert, P., and Wotawa, G.: Technical note: The Lagrangian particle
721 dispersion model FLEXPART version 6.2, *Atmospheric Chemistry and Physics*, 5, 2461-2474, 2005.
722 Stull, R.: *An Introduction to Boundary Layer Meteorology*, Kluwer Academic Publishers, Dordrecht,
723 1988.
724 Wanninkhof, R., and McGillis, W.: A cubic relationship between air-sea CO₂ exchange and wind
725 speed, *Geophysical Research Letters*, 26, 1889-1892, 10.1029/1999GL900363, 1999.
726 Yokouchi, Y., Li, H., Machida, T., Aoki, S., and Akimoto, H.: Isoprene in the marine boundary layer
727 (Southeast Asian Sea, eastern Indian Ocean, and Southern Ocean): Comparison with dimethyl sulfide
728 and bromoform, *Journal of Geophysical Research-Atmospheres*, 104, 8067-8076,
729 10.1029/1998JD100013, 1999.
730 Yokouchi, Y., Hasebe, F., Fujiwara, M., Takashima, H., Shiotani, M., Nishi, N., Kanaya, Y., Hashimoto,
731 S., Fraser, P., Toom-Sauntry, D., Mukai, H., and Nojiri, Y.: Correlations and emission ratios among
732 bromoform, dibromochloromethane, and dibromomethane in the atmosphere, *Journal of*
733 *Geophysical Research-Atmospheres*, 110, 10.1029/2005JD006303, 2005.
734 Yokouchi, Y., Osada, K., Wada, M., Hasebe, F., Agama, M., Murakami, R., Mukai, H., Nojiri, Y.,
735 Inuzuka, Y., Toom-Sauntry, D., and Fraser, P.: Global distribution and seasonal concentration change
736 of methyl iodide in the atmosphere, *Journal of Geophysical Research-Atmospheres*, 113,
737 10.1029/2008JD009861, 2008.

738